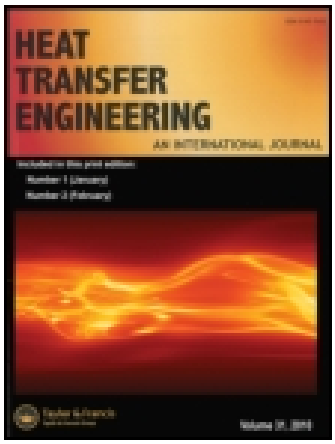
This article was downloaded by: [Imperial College London Library]
On: 20 April 2015, At: 09:17
Publisher: Taylor & Francis
Informa Ltd Registered in England and Wales Registered Number: 1072954 Registered office: Mortimer House, 37-41 Mortimer Street, London W1T 3JH, UK



Heat Transfer Engineering
Publication details, including instructions for authors and subscription information:
http://www.tandfonline.com/loi/uhte20

Optimizing the Non-Inertive-Feedback Thermofluidic Engine for the Conversion of Low-Grade Heat to Pumping Work

Karthikeyan Palanisamy[a], Aly I. Taleb[a] & Christos N. Markides[a]
[a] Clean Energy Processes (CEP) Laboratory, Department of Chemical Engineering, Imperial College London, London, United Kingdom
Accepted author version posted online: 17 Dec 2014.

CrossMark
Click for updates

To cite this article: Karthikeyan Palanisamy, Aly I. Taleb & Christos N. Markides (2015) Optimizing the Non-Inertive-Feedback Thermofluidic Engine for the Conversion of Low-Grade Heat to Pumping Work, Heat Transfer Engineering, 36:14-15, 1303-1320, DOI: 10.1080/01457632.2015.995014

To link to this article: http://dx.doi.org/10.1080/01457632.2015.995014

PLEASE SCROLL DOWN FOR ARTICLE

Taylor & Francis makes every effort to ensure the accuracy of all the information (the "Content") contained in the publications on our platform. Taylor & Francis, our agents, and our licensors make no representations or warranties whatsoever as to the accuracy, completeness, or suitability for any purpose of the Content. Versions of published Taylor & Francis and Routledge Open articles and Taylor & Francis and Routledge Open Select articles posted to institutional or subject repositories or any other third-party website are without warranty from Taylor & Francis of any kind, either expressed or implied, including, but not limited to, warranties of merchantability, fitness for a particular purpose, or non-infringement. Any opinions and views expressed in this article are the opinions and views of the authors, and are not the views of or endorsed by Taylor & Francis. The accuracy of the Content should not be relied upon and should be independently verified with primary sources of information. Taylor & Francis shall not be liable for any losses, actions, claims, proceedings, demands, costs, expenses, damages, and other liabilities whatsoever or howsoever caused arising directly or indirectly in connection with, in relation to or arising out of the use of the Content.

This article may be used for research, teaching, and private study purposes. Terms & Conditions of access and use can be found at http://www.tandfonline.com/page/terms-and-conditions

It is essential that you check the license status of any given Open and Open Select article to confirm conditions of access and use.

Heat Transfer Engineering, 36(14–15):1303–1320, 2015
Published with license by Taylor & Francis
ISSN: 0145-7632 print / 1521-0537 online
DOI: 10.1080/01457632.2015.995014

Taylor & Francis
Taylor & Francis Group

Optimizing the Non-Inertive-Feedback Thermofluidic Engine for the Conversion of Low-Grade Heat to Pumping Work

KARTHIKEYAN PALANISAMY, ALY I. TALEB, and CHRISTOS N. MARKIDES

Clean Energy Processes (CEP) Laboratory, Department of Chemical Engineering, Imperial College London, London, United Kingdom

Downloaded by [Imperial College London Library] at 09:18 20 April 2015

This paper deals with the dynamic modeling and multiparametric optimization of a thermally powered, reciprocating/oscillator fluid pumping technology known as the Non-Inertive-Feedback Thermofluidic Engine (NIFTE), with the aim of proposing pathways for the improvement of the capabilities of this technology. Analogies are drawn between the physical device and an electric circuit. All system parameters are perturbed simultaneously and independently, and configurations exhibiting the highest efficiencies, highest pumped volumetric flow rates, and lowest feedback gains (corresponding to lowest temperatures or heat inputs necessary for continuous operation) are examined. A sensitivity analysis is also undertaken. Low feedback tube resistances and inductances, low thermal resistances, and also low adiabatic volume capacitances all allow for high efficiencies and flow rates, as do somewhat elevated (relative to a preselected "nominal" design) load resistances and inductances, and displacer cylinder capacitances and inductances. The power cylinder inductance has its optimum near its selected nominal value. Generally, the power and displacer cylinder capacitances do not significantly affect the investigated performance indicators. The heat exchangers, vapor volume, and power cylinder are identified as important components that control the performance of the device. The optimal parameter values can be taken as useful indications toward the design of an improved NIFTE pumping device.

INTRODUCTION

The continuing dependency on fossil fuels for the provision of heat and power is a matter of heightened concern, with emissions from their combustion posing a threat to human health and the environment. Nevertheless, and although their availability is ultimately finite, the global demand for these primary energy resources is growing. This predicament is the main driver for intensive research in the areas of sustainable or alternative means of heat and power production. Two paths can be followed to reduce the dependency on fossil fuels: on the one hand, by developing and improving alternative or renewable energy sources, such as solar or geothermal; and on the other hand, by increasing the efficiency of conventional fossil fuel conversion, for example, through energy integration and the recovery and reuse of waste heat [1].

Non-concentrated solar and geothermal heat can be classified as low-grade heat sources, which is often understood as heat at temperatures below ∼250°C [2]. In addition, waste heat is rejected continuously and in large quantities from most industrial processes (e.g., oil refining, chemical plants, power generation), in the transport sector (e.g., motor vehicles, trains), in many commercial settings, and so on. It is therefore available abundantly and at a fraction of the cost of other energy sources. Due to the low temperature of the heat source, however, the second law of thermodynamics dictates that the theoretically

Address correspondence to Dr. Christos N. Markides, Department of Chemical Engineering, Imperial College London, South Kensington Campus, London SW7 2AZ, United Kingdom. E-mail: c.markides@imperial.ac.uk

Color versions of one or more of the figures in the article can be found online at www.tandfonline.com/uhte.

© K. Palanisamy, A. I. Taleb, and C. N. Markides. This is an Open Access article distributed under the terms of the Creative Commons Attribution License (http://creativecommons.org/licenses/by/3.0), which permits unrestricted use, distribution, and reproduction in any medium, provided the original work is properly cited. The moral rights of the named author(s) have been asserted.

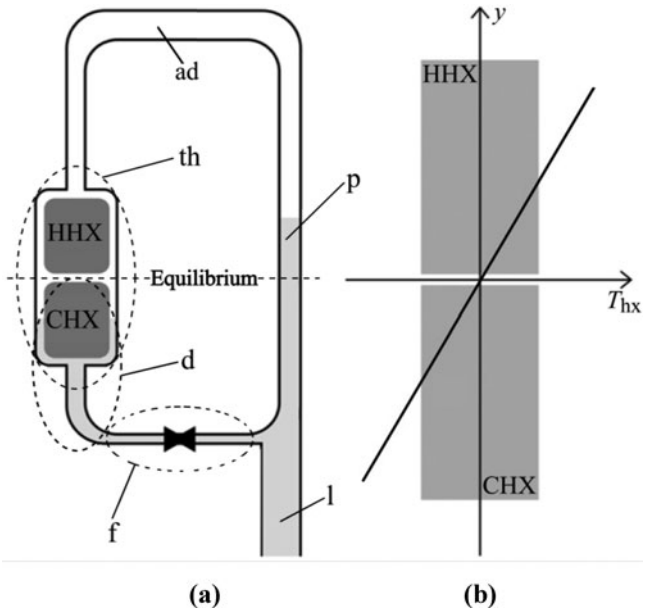


Figure 1 (a) NIFTE fluid pump schematic. The gray area represents the liquid phase and the white represents the vapor phase. Components are identified by their respective subscripts. The load line is denoted by subscript "l," the combination of hot (HHX) and cold (CHX) heat exchangers by "th," the feedback connection by "f," the power cylinder by "p," and the displacer cylinder by "d." The combined vapor space/volume above the liquid in the displacer and power cylinders is assumed to be an adiabatic chamber, "ad." The horizontal dashed line depicts the equilibrium level. (b) Temperature profile imposed in the thermal domain "th" (on the surface walls of the CHX and HHX heat exchangers) of the LTP model.

maximum thermal efficiency, or Carnot efficiency, will be intrinsically low [1, 3]. This explains why high-grade heat conversion has traditionally dominated power generation, and consequently why most conventional power generation (heat engine) systems are not suitable for the low temperature differences between the heat source and heat sink associated with low-grade heat conversion.

Investigated in the present paper is a heat engine device capable of converting low-grade heat to hydraulic work through its conversion to an oscillatory motion of a fluid. This oscillatory heat engine belongs to a class of heat engines referred to as "thermofluidic oscillators." A thermofluidic oscillator consists of a series of chambers interconnected with tubes within which a suitable working fluid is subjected to time-varying heat transfer and flow resulting in an unsteady, periodic thermodynamic cycle driven by a pair of hot and cold heat exchangers. Notably, they feature no or few mechanical moving parts. The particular type of thermofluidic oscillator investigated herein is known as the "Non-Inertive-Feedback Thermofluidic Engine" (NIFTE) [4–10], and is a two-phase oscillator within which the working fluid exists simultaneously in the liquid and vapor phases [4, 11, 12]. The cyclic evaporation (during heat addition) and condensation (during heat rejection) of the working fluid induces sustained thermodynamic (pressure, volume, temperature) oscillations, giving rise to oscillatory fluid motion, which is output as useful hydraulic work.

The NIFTE produces work in a way similar to a Fluidyne engine, which is a Stirling engine featuring liquid pistons [13, 14]. A Stirling engine, be it with liquid or solid pistons, operates by cyclically compressing and expanding the working fluid (gas) while heat is exchanged (added and removed) at different temperatures. There are no valves or other mechanical parts that control the flow, with the pressure and volume changes inducing fluid motion [15]. However, whereas in the (gas-phase cycle) Fluidyne engine there is no phase change, a fraction of the fluid in the NIFTE periodically changes phase. The benefit of employing phase change in the NIFTE is that the engine is capable of sustaining significant oscillation amplitudes and considerably higher rates of heat exchange over small temperature differences (as low as 30°C [5]) between the heat source and heat sink, while having significantly simpler and smaller heat exchangers owing to the higher heat transfer coefficients associated with phase change (compared to single-phase forced convection).

The key merits of the NIFTE are its simple construction, the lack of moving mechanical parts, low maintenance, and, hence, its low capital and operating cost. It is especially suitable for off-grid or remote-area pumping applications with low-grade solar, geothermal, or waste heat as an energy source to enhance energy and carbon savings [8].

The NIFTE is shown in Figure 1a, where the white area represents the vapor phase and the gray area represents the liquid phase of the working fluid, normally pentane [4]. Due to gravity the liquid phase is found in the lower part of the device while the vapor phase collects in the upper part in a combined vapor region that has been termed the adiabatic vapor volume ("ad"). The two main vertical cylinders in the NIFTE are known as the power cylinder ("p") and the displacer cylinder ("d"), in which the hot heat exchanger block (HHX) and cold heat exchanger block (CHX) are located. These two vertical cylinders are connected by two horizontal tubes. The connecting tube that contains the working fluid in the liquid phase is referred to as the feedback connection ("f"), while the connection that contains the working fluid in the vapor phase is referred to as the vapor connection. The feedback connection also features a valve that can be used to adjust the operation of the engine while it is running, if necessary. In addition, the power cylinder is directly connected to the load line ("l") directly below it, where the useful (displacement) work of the device is done.

Briefly describing the operation of the NIFTE, the schematic representation in Figure 1a shows the liquid level (vapor–liquid interface) in the displacer cylinder ("d") of the device to be in contact with the CHX block. At this point the working fluid (vapor phase) is condensing over the uncovered cold CHX surface, which is at a lower temperature than the condensation temperature of the working fluid at the operation pressure. This reduces the mass of vapor and the pressure in the adiabatic vapor volume ("ad"), which in turn causes the liquid level in the power cylinder ("p") to rise. As this occurs, the hydrostatic pressure difference developing between the two arms of the U-tube arrangement featuring the power and displacer cylinders, and the

Downloaded by [Imperial College London Library] at 09:18 20 April 2015

connecting feedback connection, increases and eventually becomes large enough first to decelerate and then to reverse this motion of the liquid levels in the power and displacer cylinders, causing the levels to return to equilibrium (horizontal dashed line in Figure 1a) and then to overshoot this. Consequently, the liquid level in the displacer cylinder contacts the hot surface of the HHX block, which causes the working fluid (liquid phase) to evaporate. This gives rise to an increased mass of vapor and increased pressure in the adiabatic vapor volume that displaces the liquid level downward in the power cylinder. Eventually, the hydrostatic pressure difference between the liquid columns in the power and displacer cylinders causes the levels to return to equilibrium (due to processes that are opposite to those in the first half of the cycle) and then to overshoot this, at which point the NIFTE returns to the position shown in Figure 1a. This process repeats, leading to sustained oscillations from the stationary boundary conditions in the heat exchangers. The pressure and volume oscillations in the power cylinder are of great importance as they also affect the oscillations in the load ("l") where (hydraulic; fluid pumping) work is done.

In previous efforts of modeling the NIFTE device [4–9], the authors developed a set of spatially lumped and linearized submodels, with each submodel describing separately the dominant thermal and/or fluid process identified as taking place in a particular compartment or subsection of the NIFTE device. After using electrical analogies, as is the convention in this field, the resulting differential equations governing the important processes undergone in each of the spatial regions of the NIFTE were represented by passive electrical components, such as resistors, capacitors, and inductors. By connecting the submodels in the same way that the corresponding subsections are connected in the physical manifestation of the NIFTE, electrical circuit model analogies of the entire device were constructed.

Figure 2 shows two separate attempts at modeling the NIFTE, identical in all aspects other than the modeling of the heat exchangers in the thermal domain: (a) the linear temperature profile (LTP) model, which imposes a time-invariant, constant temperature gradient along the vertical height of the heat exchanger block walls; and (b) the dynamic heat exchanger (DHX) model, which allows the temperature of the segment of the heat exchanger block in contact with the liquid–vapor interface to time-vary (in response to an energy balance) while imposing a time-invariant heat gradient along the vertical height of the heat exchanger blocks [7].

The overall NIFTE system is fully described by 10 independent parameters in the case of the LTP model, or 11 independent parameters in the case of the DHX model. In references [4–9] these parameters were evaluated for the geometric configuration and fluids used in an early NIFTE water-pump prototype presented in references [4, 11, and 12], and are denoted here as the "nominal" values of these parameters. Subsequently, individual parameters were perturbed within a reasonable range from their nominal values while all other parameters were kept constant, in order to investigate the influence of each parameter on the operation and performance of the system, especially the oscillation

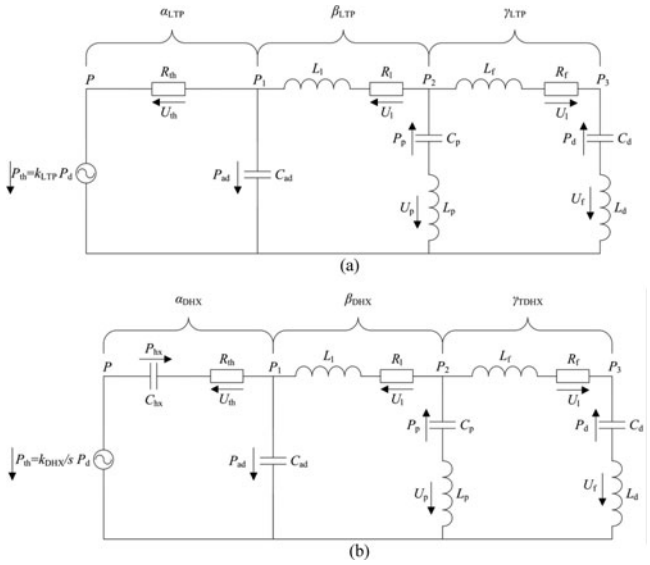


Figure 2 Electrical circuit representations of the NIFTE for the (a) LTP and (b) DHX models, where k_j is the feedback gain for model "j," R_i is a resistance, C_i is a capacitance, L_i is an inductance, P_i is a pressure and U_i is a volumetric flow rate. Subscript "hx" denotes the heat exchangers, "th" the thermal domain, "ad" the adiabatic vapor domain, "l" the load line, "p" the power cylinder, "d" the displacer cylinder (containing the two heat exchangers), and "f" the feedback connection.

frequency and exergy efficiency. In this paper, we present a more comprehensive multiparametric study that allows all variables to be perturbed simultaneously and consider the capabilities of the NIFTE device within this entire design space. This results in more than 200 million different combinations (configurations), which are investigated for the highest efficiency, highest pumped flow rate and lowest gain. Additionally, the sensitivity of these three performance indicators to the design parameters (geometrical, fluid selection, and operational) of the NIFTE pump is considered.

MODELING METHODOLOGY

Electrical Analogies

The approach taken in modeling the NIFTE device is explained in detail in references [5–9], where these models are also validated against a range of experimental data from an early-stage NIFTE water-pump prototype [4, 11, 12]. Here, we summarize the main points of this approach. Each electrical component in the NIFTE RLC circuit represents a submodel (i.e., section) of the NIFTE device, whereby (i) resistors describe heat transfer and viscous/form drag effects (both associated with pure exergetic dissipation and loss); (ii) capacitors describe gravitational/hydrostatic and vapor compressibility effects; and (iii) inductors describe the inertia experienced by oscillating liquid columns/flows. This approach requires analogies to be made between the physical and the electrical domains. As such, a pressure (P_i) difference across a physical NIFTE device component in the fluid domain, in region "i" (e.g., i =

Downloaded by [Imperial College London Library] at 09:18 20 April 2015

Downloaded by [Imperial College London Library] at 09:18 20 April 2015

"f," "l," "d," "p," "ad"), is represented by a voltage (E_i) difference across an equivalent analogous electrical component, while the volumetric flow rate (U_i) through the same physical component is represented by the current (I_i) flowing through the corresponding electrical component. Similarly, in the thermal domain, in region "i" (e.g., "th," "hx"), a temperature (T_i) difference across a physical NIFTE component is represented by a voltage (E_i) drop across an equivalent electrical component, and the resulting entropy flow rate ($\dot{S}_i$) through the physical component is represented by a current (I_i) flowing through the electrical component.

The preceding identification requires that each domain is characterized by a single dominant thermal or fluid transport process. The aim is then to develop linearized and spatially lumped submodels that describe the dynamic thermal or fluid processes undergone within each domain. The linearization of a governing equation for a thermal or fluid transport process allows for a comparison to be made with linear, passive electrical components.

The dynamic equation describing a pure resistor R_i is given by Ohm's law, $E_i \equiv R_i I_i$, where the voltage across the resistor E_i is directly proportional to the current through it, I_i. The dynamic equation describing an inductor L_i arises from Faraday's law as $E_i \equiv L_i \frac{dI_i}{dt} \Rightarrow E_i = sL_i I_i$, where the right-hand-side expression shows the governing equation for an inductor in the Laplace domain and the Laplace variable s represents a time derivative. Finally, the dynamic equation describing a capacitor C_i is derived similarly from Gauss's law as $\frac{dE_i}{dt} \equiv \frac{I_i}{C_i} \Rightarrow E_i = \frac{1}{sC_i} I_i$.

Fluid Domain Modeling

The resistance arising in a laminar pipe flow at low pulsation frequencies can be calculated using Poiseuille's flow law, where the concept of frictional drag comes into the picture. In this case, the pressure difference and the resistance across a tube of length l are:

$$\Delta P = \frac{128\,\mu l}{\pi d^4} U \equiv RU \tag{1}$$

$$R = \frac{128\,\mu l}{\pi d^4} \tag{2}$$

The inertial (inductive) contributions can be introduced via Newton's second law of motion, which states that a net resultant force F on a body of constant mass m is equal to the rate of change of its linear momentum. Thus, for the liquid in a tube one can write:

$$F = \frac{m}{A}\frac{\mathrm{d}U}{\mathrm{d}t} \tag{3}$$

where the mass of fluid in the tube m is assumed to remain constant with time. In order to relate Eq. (3) to electrical components, this equation is written in terms of pressure as:

$$\Delta P = \frac{F}{A} = \frac{\rho_{\mathrm{wf}} l}{A}\frac{\mathrm{d}U}{\mathrm{d}t} \equiv L\frac{\mathrm{d}U}{\mathrm{d}t} \Rightarrow \Delta P = sLU \tag{4}$$

where s is the Laplace variable and l is the length of the tube occupied by the liquid.

Comparing Eq. (4) to the characteristic equation for an inductor and making the same analogies between the fluid domain and electrical domain, the inductance due to inertia in the feedback tube is:

$$L = \frac{\rho_{\mathrm{wf}} l}{A} \tag{5}$$

To account for capacitive effects, the hydrostatic pressure (difference) at the bottom of a vertical tube ΔP can be approximated to first order by:

$$\Delta P = \rho_{\mathrm{wf}} g \frac{V}{A} \tag{6}$$

for a given volume of liquid in the tube V, where g is the gravitational acceleration constant and A is the cross-sectional area of the tube. To express this relation in electrical components, Eq. (6) is differentiated with respect to time, giving:

$$\mathcal{L}\left\{\frac{\mathrm{d}(\Delta P)}{\mathrm{d}t}\right\} = s(\Delta P) = \frac{\rho_{\mathrm{wf}} g}{A}\frac{\mathrm{d}V}{\mathrm{d}t} = \frac{\rho_{\mathrm{wf}} g}{A} U \tag{7}$$

where s is the Laplace variable and U is the volumetric flow rate into the tube, such that the capacitance due to hydrostatic pressure in the tube is:

$$C = \frac{A}{\rho_{\mathrm{wf}} g} \tag{8}$$

The expressions for the inductances, resistances, and capacitances of the power cylinder ("p"), displacer cylinder ("d"), load line ("l"), and feedback connection ("f") can be found in Table 2 (shown later).

In the (nominally) adiabatic vapor volume, assuming the processes undergone by the working fluid (in the vapor phase) is adiabatic and reversible (i.e., isentropic), the vapor compression and expansion of this volume can be described by:

$$P_{\mathrm{ad}} V_{\mathrm{ad}}^{\gamma} = \text{const.} \tag{9}$$

where P_{ad} and V_{ad} are the time-varying pressure and volume of the vapor, and γ is the heat capacity ratio of the working fluid. The pressure and volume can be expressed as the sum of the time-averaged mean and the fluctuation about this mean, that

Table 1 Important transfer functions for the two models (LTP, DHX) in Figure 2

NIFTE model	$\alpha_i = \frac{P_1}{P}$	$\beta_i = \frac{P_2}{P_1}$	$\gamma_i = \frac{P_3}{P_2}$
i = LTP	$1 - \frac{R_{\mathrm{th}}}{Z_{\mathrm{TOT,LTP}}}$	$1 - Z_{\mathrm{l}}\left(\frac{Z_{\mathrm{TOT,LTP}}}{\alpha_{\mathrm{LTP}}} - sC_{\mathrm{ad}}\right)$	$\frac{1}{1+Z_{\mathrm{f}}/Z_{\mathrm{d}}}$
i = DHX	$1 - \frac{R_{\mathrm{th}} + \frac{1}{sC_{\mathrm{hx}}}}{Z_{\mathrm{TOT,DHX}}}$	$1 - Z_{\mathrm{l}}\left(\frac{Z_{\mathrm{TOT,DHX}}}{\alpha_{\mathrm{DHX}}} - sC_{\mathrm{ad}}\right)$	$\frac{1}{1+Z_{\mathrm{f}}/Z_{\mathrm{d}}}$

Downloaded by [Imperial College London Library] at 09:18 20 April 2015

Table 2 Electrical analogies in the two NIFTE models linear temperature profile (LTP) and dynamic heat exchanger (DHX), and definitions of all R, C, and L parameters

Electrical element	Thermal-fluid effect	Parameter expression
Resistance (R)	Heat exchanger thermal resistance	$R_{\text{th}} = \frac{\rho_{\text{g},0}\Delta s_{\text{fg}} T_0}{hS\left(\frac{\text{d}T}{\text{d}P}\right)_{\text{sat}}}$
	Load line flow resistance	$R_{\text{l}} = \frac{128\mu_{\text{w}} l_{\text{l}}}{\pi d_{\text{l}}^4}$
	Feedback connection flow resistance	$R_{\text{f}} = \frac{128\mu_{\text{pen}} l_{\text{f}}}{\pi d_{\text{f}}^4}$
Capacitance (C)	Adiabatic vapor volume compressibility	$C_{\text{ad}} = \frac{V_{\text{eq}}}{\gamma P_{\text{eq}}}$
	Power cylinder hydrostatic capacitance	$C_{\text{p}} = \frac{A_{\text{P}}}{\rho_{\text{pen}} g}$
	Displacer cylinder hydrostatic capacitance	$C_{\text{d}} = \frac{A_{\text{d}}}{\rho_{\text{pen}} g}$
	Heat exchanger thermal storage capacitance	$C_{\text{hx}} = \frac{mc\left(\frac{\text{d}T}{\text{d}P}\right)_{\text{sat}}}{\rho_{\text{g},0}\Delta s_{\text{fg}} T}$
Inductance (L)	Load line inertia	$L_{\text{l}} = \frac{\rho_{\text{w}} l_{\text{l}}}{A_{\text{l}}}$
	Power cylinder liquid column inertia	$L_{\text{p}} = \frac{\rho_{\text{pen}} l_{\text{p}}}{A_{\text{p}}}$
	Displacer cylinder liquid column inertia	$L_{\text{d}} = \frac{\rho_{\text{pen}} l_{\text{d}}}{A_{\text{d}}}$
	Feedback tube inertia	$L_{\text{f}} = \frac{\rho_{\text{pen}} l_{\text{f}}}{A_{\text{f}}}$

is, $P_{\text{ad}} = \bar{P}_{\text{ad}} + P'_{\text{ad}}$ and $V_{\text{ad}} = \bar{V}_{\text{ad}} + V'_{\text{ad}}$. Assuming there are only small fluctuations and taking the time derivative of Eq. (9) gives:

$$\frac{1}{\bar{P}_{\text{ad}}}\frac{\text{d}\bar{P}_{\text{ad}}}{\text{d}t} + \frac{\gamma}{\bar{V}_{\text{ad}}}\frac{\text{d}\bar{V}_{\text{ad}}}{\text{d}t} = 0 \tag{10}$$

The time-averaged pressure is taken to be the equilibrium pressure, P_0, and time-averaged volume is taken to be the equilibrium volume, $V_{\text{g},0}$, such that $P_0 \equiv \bar{P}_{\text{ad}}$ and $V_{\text{g},0} \equiv \bar{V}_{\text{ad}}$, and:

$$\frac{1}{\bar{P}_{\text{ad}}}\frac{\text{d}\bar{P}_{\text{ad}}}{\text{d}t} + \frac{\gamma}{\bar{V}_{\text{ad}}}\frac{\text{d}\bar{V}_{\text{ad}}}{\text{d}t} = 0 \tag{11}$$

where U_{ad} is the rate of reduction of the adiabatic vapor volume, or the net volumetric flow rate into the adiabatic vapor volume, defined as $-\text{d}V_{\text{ad}}/\text{d}t$. Comparing Eq. (11) to the equation for a capacitor, the capacitance due to adiabatic compression and expansion is:

$$C_{\text{ad}} = \frac{V_{\text{g},0}}{\gamma P_0} \tag{12}$$

The derivations of the electrical components just described are given in detail in references [5–9].

Thermal and Fluid Domain Coupling

To link the thermal domain processes to the ones taking place in the fluid domain, two coupling equations are required: one between entropy flow and volumetric flow, and the other between temperature and pressure [5–9]. The large change in volume/density that takes place during phase change leads to the following coupling equation between the entropy flow rate $\dot{S}_{\text{th}}$ due to heat transfer and the volumetric flow rate U_{th}:

$$\dot{S}_{\text{th}} = \rho_{\text{g},0}\Delta s_{\text{fg}} U_{\text{th}} \tag{13}$$

where $\rho_{\text{g},0}$ is the time-averaged density of the working fluid in the vapor phase and Δs_{fg} is the entropy change due to vaporization.

Further, assuming that the thermal processes are governed by phase change with small perturbations about a certain time-mean saturation temperature T_0 (and pressure P_0), the coupling equation between temperature and pressure is:

$$T_i = \left(\frac{\text{d}T}{\text{d}P}\right)_{\text{sat}} P_i \tag{14}$$

where $(\text{d}T/\text{d}P)_{\text{sat}}$ is the change in temperature with pressure along the saturation curve of the working fluid at the equilibrium point found from the Clausius–Clapeyron relation.

Thermal Domain Modeling

In order to model the thermal interaction between the heat exchangers and the working fluid, it is assumed that this is dominated by convective heat transfer, for which all heat transferred from/to the heat exchanger blocks $\dot{Q}$ goes into the phase change of the working fluid with an associated entropy flow rate $\dot{S}_{\text{th}}$:

$$\frac{\dot{Q}}{T_0} = \dot{S}_{\text{th}} = \frac{hS}{T_0}(T_{\text{hx}} - T_{\text{ad}}) \tag{15}$$

where h is the convective heat transfer coefficient, S is the surface area of the heat exchanger blocks involved in the phase-change heat transfer, T_{ad} is the temperature of the working fluid, and T_{hx} is the temperature of the heat exchangers. As before, T_0 is the mean, time-averaged, saturation temperature for the working fluid, about which the temperatures fluctuate. This temperature is assumed to be equal to the mean temperature of the hot and cold heat exchangers, as well as the time-averaged temperature of the working fluid in the vapor phase, such that $T_0 \equiv \bar{T}_{\text{hx}} = \bar{T}_{\text{ad}}$.

Substituting the two coupling equations that link the thermal domain to the fluid domain, Eq. (13) and Eq. (14), into the heat transfer equation, Eq. (15) can be written in the fluid domain as:

$$P_{\text{th}} - P_{\text{ad}} = \frac{\rho_{\text{g},0} T_0 \Delta s_{\text{fg}}}{hS\left(\frac{\text{d}T}{\text{d}P}\right)_{\text{sat}}} U_{\text{th}} = R_{\text{th}} U_{\text{th}} \tag{16}$$

Comparing Eq. (5) to Ohm's law, the thermal resistance between the heat exchanger blocks and the working fluid in the

LTP model is:

$$R_{\text{th}} = \frac{\rho_{g,0} T_0 \Delta s_{\text{fg}}}{hS \left(\frac{dT}{dP}\right)_{\text{sat}}} \tag{17}$$

Linear Temperature Profile (LTP) Thermal Domain Model

The linear temperature profile (LTP) heat exchanger model [4–9] imposes a static, linear temperature profile in the vertical direction on the surface of the heat exchanger blocks, as shown in Figure 1b. The equation employed to describe the phase-change convective heat transfer process between the heat exchangers and the working fluid is:

$$\dot{Q} = hS\left[T_{\text{hx}}(y) - T_{\text{ad}}\right] \tag{18}$$

where $\dot{Q}$ is the heat transfer rate, h the (constant) heat transfer coefficient, S the (constant) surface area available to phase-change heat transfer, and T_{hx} and T_{ad} the heat exchanger block and working fluid temperatures at the vicinity of phase change. The relation $T_{\text{hx}} \propto y$ in Figure 1b (or $P_{\text{th}} = k_{\text{LTP}} P_{\text{d}}$ in Figure 2a) describes the heat exchanger block surface/wall temperature as a function of the height of the vapor–liquid interface in the displacer cylinder. The feedback constant k_{LTP} is proportional to the temperature gradient in the heat exchanger blocks $\Delta T_{\text{HX}}/\Delta y$. The value of this gradient at marginal stability is related to the minimum required temperature difference to achieve sustained oscillations.

The total impedance of the LTP circuit in Figure 2a relates the input pressure P_{th} to the input flow rate U_{th}, and is obtained by adding contributions from all impedances in the circuit. The result of this working gives:

$$Z_{\text{TOT,LTP}} \equiv \frac{P_{\text{th}}}{U_{\text{th}}} = R_{\text{th}} + (sC_{\text{ad}} + (Z_{\text{l}} + ((Z_{\text{f}} + Z_{\text{d}})^{-1} + Z_{\text{p}}^{-1})^{-1})^{-1})^{-1} \tag{19}$$

where $Z_{\text{f}} = R_{\text{f}} + sL_f$, $Z_{\text{d}} = sL_{\text{d}} + 1/sC_{\text{d}}$, $Z_{\text{p}} = sL_{\text{p}} + 1/sC_{\text{p}}$, and $Z_{\text{l}} = R_{\text{l}} + sL_{\text{l}}$. These impedance definitions also apply to the revised models in the following two subsections. Expressions for the three important transfer functions that appear in Figure 2a, namely, α_{LTP}, β_{LTP} and γ_{LTP}, can be found in Table 1.

Dynamic Heat Exchanger (DHX) Thermal Domain Model

This model [7, 8] accounts for the ability of the heat exchanger blocks to store and release thermal energy. After ignoring external heat losses, the heat transfer in the heat exchanger blocks is assumed to obey:

$$\dot{Q}_{\text{HX}} - hS\left[T_{\text{hx}}(y) - T_{\text{ad}}\right] = mc\left(\frac{dT_{\text{hx}}}{dt}\right) \tag{20}$$

where $\dot{Q}_{\text{HX}}$ is the power to/from the HHX/CHX heat exchanger blocks, m the solid block mass taking active part in the heat transfer, c their specific heat capacity, and $T_{\text{hx}}(y)$ the instantaneous heat exchanger wall temperature at the vertical location of the liquid–vapor interface. As in the LTP model, h is the heat transfer coefficient, S is the heat transfer surface area, and T_{ad} is the temperature of the working fluid. Using the coupling equations defined in Eqs. (13) and (14), the following relation can be derived from Eq. (20):

$$U_{\text{th}} = C_{\text{hx}} \frac{dP_{\text{hx}}}{dt} + \frac{1}{R_{\text{th}}}\left(P_{\text{th}} - P_{\text{ad}}\right) \tag{21}$$

where the heat exchanger thermal storage capacitance is:

$$C_{\text{hx}} = \frac{mc\left(\frac{dT}{dP}\right)_{\text{sat}}}{\rho_{g,0} \Delta s_{\text{fg}} T_0} \tag{22}$$

The relation $P_{\text{th}} = k_{\text{DHX}} P_{\text{d}}/s$ (in Figure 2b) describes the heat transfer from the heat exchanger blocks as a function of the height of the vapor–liquid interface in the displacer cylinder. The feedback constant k_{DHX} is proportional to the heat power gradient in the heat exchanger blocks $\Delta Q_{\text{HX}}/\Delta y$. The value of this gradient at marginal stability is related to the minimum required heat power input to achieve sustained oscillations.

This parameter, in combination with the thermal resistance R_{th}, describes the characteristics of the heat exchangers and the heat transfer processes. In particular, the heat exchanger capacitance C_{hx} is a measure of the capacity of the heat exchanger to store and release thermal energy, and the thermal resistance R_{th} indicates the dissipation of thermal energy during the transfer of heat from the heat exchanger to the working fluid.

The electric circuit representation of this heat exchange model of the NIFTE can be seen in Figure 2b. The total impedance of the circuit in Figure 2b relates the input pressure P_{th} to the input flow rate U_{th}, and is obtained by adding contributions from all impedances in the circuit:

$$Z_{\text{TOT,DHX}} \equiv \frac{P_{\text{th}}}{U_{\text{th}}} = (sC_{\text{hx}})^{-1} + R_{\text{th}} + (sC_{\text{ad}} + (Z_{\text{l}} + ((Z_{\text{f}} + Z_{\text{d}})^{-1} + Z_{\text{p}}^{-1})^{-1})^{-1})^{-1} \tag{23}$$

The three transfer functions in Figure 2b, namely, α_{DHX}, β_{DHX}, and γ_{DHX}, which are used to evaluate quantities of interest such as device efficiencies, are given in Table 1.

In Markides et al. [9] a nonlinear temperature profile (saturation) was imposed along the heat exchanger walls in order to capture and examine the actual dynamic behavior of the NIFTE that is, in fact, undergoing limit cycle operation. A nonlinear temperature profile was not considered in the investigation presented in this present paper; however, a consideration of this model would be a useful and natural extension of the present work.

Downloaded by [Imperial College London Library] at 09:18 20 April 2015

Table 3 Calculated nominal values and corresponding investigated ranges for the RLC parameters in Table 2

Electrical element	Nominal value	Investigated range	Number of points in range	Units
R_{th}	5.02×10^{8}	3.13×10^{7} to 7.20×10^{9}	9	kg/m^4-s
R_l	4.08×10^{6}	4.08×10^{0} to 1.51×10^{10}	5	kg/m^4-s
R_f	2.13×10^{6}	7.10×10^{1} to 4.44×10^{9}	9	kg/m^4-s
C_{ad}	1.76×10^{-9}	9.84×10^{-11} to 1.40×10^{-7}	9	m^4-s ^{2}/kg
C_p	7.43×10^{-8}	3.22×10^{-9} to 1.29×10^{-6}	9	m^4-s ^{2}/kg
C_d	7.35×10^{-8}	1.44×10^{-8} to 1.20×10^{-6}	9	m^4-s ^{2}/kg
C_{hx}	2.85×10^{-8}	3.25×10^{-10} to 3.82×10^{-6}	7	m^4-s ^{2}/kg
L_l	1.27×10^{7}	1.27×10^{3} to 4.24×10^{9}	5	kg/m^4
L_p	3.77×10^{5}	7.90×10^{3} to 3.16×10^{7}	9	kg/m^4
L_f	4.74×10^{6}	1.57×10^{4} to 3.95×10^{8}	9	kg/m^4
L_d	1.80×10^{5}	8.50×10^{3} to 7.01×10^{6}	9	kg/m^4

Downloaded by [Imperial College London Library] at 09:18 20 April 2015

MODEL PARAMETERS

The expressions used to evaluate each electrical (RLC) device parameter in both the LTP and DHX models of the NIFTE can be found in Table 2. To carry out the present multiparametric optimization study, each parameter was first evaluated based on a nominal value corresponding to an existing device prototype [4, 11, 12], and then perturbed over the whole parameter space about this value while staying within the confines of a physically acceptable configuration [5–8]. The nominal values and investigated ranges are stated in Table 3. The values used here are the same as those of reference [9].

Marginal Stability and Gain

Three types of oscillatory responses can be exhibited by a linear system: stable oscillations that decay exponentially, marginally stable oscillations that persist with constant amplitude, and unstable oscillations that grow exponentially [16]. The continuous oscillations observed during operation in the actual NIFTE prototype can be investigated, at least to first order, by observing the simplified linear representations of this device at marginal stability, as proposed by the various models. In this work, the frequency at which marginal stability occurs is used to evaluate all performance characteristics of interest.

The stability of a linear system can be found from the closed-loop transfer function $C(s) = G(s)/[1 + kG(s)]$, where $G(s)$ is the forward transfer function relating the input P_{th} to the output P_d, found from the electrical circuits in Figure 2, and k is the feedback gain that relates P_d to P_{th}. For the LTP and DHX models, $k = k_{LTP}$ and $k = k_{DHX}/s$, respectively [7, 8]. The stability of each system at a given gain k can be investigated by observing the poles of the closed-loop transfer function. Marginal stability occurs when one pole pair lies on the imaginary axis and all others have negative real parts. A mathematical solver using an iterative method was used to calculate the marginal stability frequency and feedback gain.

Device Exergy Efficiency

A quantity of great interest for heat engines is their efficiency, of which there are several definitions [5, 17]. The exergy efficiency is the thermal efficiency of a heat engine relative to the Carnot efficiency at the same source/sink conditions [5, 6, 18]. The thermal efficiency of the NIFTE is inherently low, due to the fact that it is converting low-grade heat, so the exergy efficiency is a more useful quantity to evaluate performance:

$$\eta_{ex} = \frac{\overline{P_l(t)\,U_l(t)}}{\overline{T_{hx}(t)\,\dot{S}_{th}(t)}} = \frac{\overline{P_l(t)\,U_l(t)}}{\overline{P_{th}(t)\,U_{th}(t)}} = \left|\frac{P_l}{P_{th}}\right|^2 \frac{\mathrm{Re}\{1/Z_l\}}{\mathrm{Re}\{1/Z_{TOT}\}} \tag{24}$$

where T_{hx} is the heat exchanger temperature at the locality of phase change, $\dot{S}_{th}$ the entropy input to the system due to the heat transfer associated with the phase change, P_l and P_{th} the load and input pressures, respectively, and U_l and U_{th} the flow rate in the load and input flow rate to the adiabatic volume due to phase change, respectively. Further details on the exergy efficiency can be found in references [4, 6] and an extensive discussion in reference [5].

Interrelation Between RLC Parameters

Each parameter has nine data points within the investigated ranges stated in Table 3. However, the load parameters R_l and L_l only have five data points and the heat exchanger capacitance C_{hx} from the DHX model has seven. Several combinations of specific parameters are unrealistic, as they would lead to impossible geometrical configurations. For example, for a given density, the smallest displacer cylinder capacitance C_d in the range corresponds to a diameter of 0.014 m. If we combine this minimum capacitance with the minimum displacer cylinder inductance, this would correspond to a length of the displacer cylinder of $l_d = L_{d,min}\pi d_d^2/4\rho = 0.0013$ m. This can be interpreted as an impossible geometric configuration, and hence, it is an unnecessary computational burden to consider such cases.

Ranges for the products C_dL_d, C_pL_p, and R_f/L_f can be calculated from:

Table 4 Interrelation and calculated ranges using the data from Table 2 and Table 3

Physical component	Geometrical dimension range	Interrelation	Range constraint
Feedback connection ("f")	$d_f = 0.001$ to 0.05 m	$\frac{R_f}{L_f} = \frac{32\mu_{pen}}{\rho_{pen} d_f^2}$	4.49×10^{-3} to 11.2
Feedback connection ("f")	$l_f = 0.05$ to 0.5 m	$\frac{R_f}{L_f^2} = \frac{8\mu_{pen}\pi}{\rho_{pen}^2 l_f}$	2.84×10^{-8} to 2.84×10^{-7}
Power cylinder ("p")	$l_p = 0.02$ to 2 m	$L_p C_p = \frac{l_p}{g}$	2.04×10^{-3} to 0.204
Displacer cylinder ("d")	$l_d = 0.2$ to 2 m	$L_d C_d = \frac{l_d}{g}$	2.04×10^{-2} to 0.204

$$\begin{aligned} C_d L_d &= \frac{A_d}{\rho_{wf} g}\frac{\rho_{wf} l_d}{A_d} = \frac{l_d}{g} \\ C_p L_p &= \frac{A_p}{\rho_{wf} g}\frac{\rho_{wf} l_p}{A_p} = \frac{l_p}{g} \\ \frac{R_f}{L_f} &= \frac{32\,\mu_{wf}}{\rho_{wf} d_f^2} \\ \frac{R_f}{L_f^2} &= \frac{8\,\pi\mu_{wf}}{\rho_{wf}^2 l_f} \end{aligned} \tag{25}$$

The values of these product ranges determine the possible combinations of C_d with L_d, C_p with L_p, and R_f with L_f. Substituting the known ranges of values of the physical dimensions (l_d from 0.2 m to 2 m; l_p from 0.02 m to 2 m; l_f from 0.05 m to 0.5 m; and d_f from 0.001 m to 0.05 m) imposes constraints on the ranges of the interrelations. The interrelations between the components and their range constraints are stated in Table 4. After excluding the unrealistic cases, the total number of combinations of parameters is reduced from more than 200 million to around 3.5 million for the LTP model and from more than 1.5 billion to about 4 million for the DHX model. Table 6 (shown later) lists the exact number of possible combinations before and after the exclusion of geometrically unrealistic combinations.

Replacing the Power and Displacer Cylinders by Spiral Tubes

There is potential for increasing the exergy efficiency of the NIFTE by increasing the inductances and capacitances of the power and displacer cylinder. Referring to the equations for C_d, C_p, L_d, and L_p (see Table 2), only an increase in the diameter d will lead to an increase of the capacitance; this will in turn, however, reduce the inductance. To increase the inductance (or keep it constant), the length l of the cylinder must increase. Doubling the diameter, for example, requires a fourfold increase of the length. This may result in unrealistically long tubes, which lead to the NIFTE acquiring unfavorably large dimensions. It is noted here that, due to the (relatively) low thermal efficiency of the NIFTE, the engine is only cost-effective for small-scale, low-cost applications [4]. This issue can be circumvented by designing the power or displacer cylinders in spiral form. In this way, the lengths of the cylinders can be increased, without affecting the size of the other components.

Let us consider the displacer cylinder as being uniformly coiled, where l_d is the total length of the tube and h_d is the vertical height as depicted in Figure 3. The hydrostatic (gauge) pressure at the bottom of the tube P_d can be approximated to first order by:

$$\frac{dP_d}{dt} = \rho_{wf} g \frac{dh_d}{dt} = \frac{1}{C_d} U_d = \frac{1}{C_d} A_d \frac{dl_d}{dt} \tag{26}$$

which gives us the value of the capacitance of the coiled displacer cylinder as:

$$C_d = \frac{A_d}{\rho_{wf} g}\frac{dl_d}{dh_d} = \frac{A_d}{\rho_{wf} g}\frac{l_d}{h_d} \tag{27}$$

where $dl_d/dh_d = l_d/h_d$ for a uniformly coiled tube and l/h is the (constant) "coiling factor."

Equation (5) illustrates that the value of the capacitance can be adjusted by coiling, which can be varied by changing the vertical height h_d, that is, by varying the coiling angle. Coiling can be introduced only in the power ("p") and displacer ("d") cylinders. The electrical analogy expressions for spiral power and displacer cylinder capacitances are $C_p^* = A_p l_p/\rho_{wf} g h_p$ and $C_d^* = A_d l_d/\rho_{wf} g h_d$, respectively. In this paper, the asterisk denotes the presence of a spiral tube in the displacer and power cylinders.

In this work, the coiling factor was set to 10, and the parameter combinations over the newly expanded range, permitted by using coiling, are given in Table 5. For a given length of tube, coiling can alter only the capacitance of the component. Note that coiling does not actually expand the ranges of the parameters but rather the ranges for the geometry governing those parameters. We have kept the parameters the same in both cases. Coiling allows us, thus, to use combinations of parameters that previously would have resulted in geometrical impossibilities. The coiled case more than doubles the number of possible

Table 5 Interrelation and calculated constraint ranges of spiral cylinders

Physical component	Geometrical dimension range	Interrelation	Range constraint
Power cylinder ("p")	$l_p = 0.02$ to 2 m; coiling factor $l_p/h_p = 10$	$L_p C_p^* = \frac{l_p^2}{g h_p}$	2.04×10^{-3} to 2.04
Displacer cylinder ("d")	$l_d = 0.2$ to 2 m; coiling factor $l_d/h_d = 10$	$L_d C_d^* = \frac{l_d^2}{g h_d}$	2.04×10^{-2} to 2.04

Downloaded by [Imperial College London Library] at 09:18 20 April 2015

Table 6 Number of combinations of different RLC parameters before and after exclusion of geometrically unrealistic combinations

	LTP		DHX	
	Noncoiled	Coiled	Noncoiled	Coiled
Total number of combinations	2.15×10^8		1.51×10^9	
Number of geometrically realistic combinations	3.55×10^6	7.82×10^6	4.03×10^6	9.11×10^6
Number of combinations of interest, which exhibit high efficiencies or flow rates, or low gains	3.55×10^5	7.82×10^5	4.03×10^5	9.11×10^5

Note: The last row corresponds to the number of NIFTE configurations in the subsets containing the RLC parameter combinations that yield the highest exergy efficiencies (top 10%), highest flow rates (top 10%), or lowest feedback gains (bottom 10%).

combinations compared to the non-coiled case. For the exact numbers, refer to Table 6.

Multiparametric Optimization

After excluding the geometrically unrealistic parameter combinations described in the previous two sections, the optimal parameter values, within the ranges listed in Table 3, are calculated according to three different criteria: high exergy efficiency, high volumetric flow rate, and low feedback gain. High pumped flow rates are a desirable goal, given that the technology is envisaged primarily as a fluid pumping device. From the sections describing the heat exchanger models we also know that the feedback gain k in the LTP model is proportional to the temperature gradient in the heat exchanger $\mathrm{d}T_{\mathrm{hx}}/\mathrm{d}y$, and proportional to the power gradient $\mathrm{d}\dot{Q}_{\mathrm{hx}}/\mathrm{d}y$ in the DHX model. Optimization of the NIFTE requires the pump to be designed for low temperature differences or low power gradients in the heat exchangers, which indirectly points to the lowering of the power consumption for operating the pump and to the ability to convert low-grade heat.

The exergy efficiency, the frequency, and the feedback gain are calculated for all geometrically realistic parameter combinations. In addition, for a given thermally driven pumping application that imposes a fixed pumping pressure across the NIFTE device and that is associated with fixed external heat source and sink temperatures, the pumped volumetric flow rate per unit heat input to the device is proportional to the product of the exergy efficiency and the frequency. Subsequently, three subsets of parameter combinations are extracted that result in the highest 10% of efficiencies, the highest 10% of pumped flow rates per unit heat input (equivalent to the product of efficiency and frequency) and the lowest 10% of feedback gains. The frequency of occurrence of the different values (i.e., data points) of each parameter is then determined for these three subsets. This is done by counting the number of occurrences of each parameter value (or data point) in a particular optimal subset (e.g., top 10% of efficiencies) and dividing this number by the total number of combinations in that subset (the exact totals can be found in the last row of Table 6). In this way we obtain the relative probability that a specific parameter value will result in a high efficiency, high flow rate or low feedback gain NIFTE configuration.

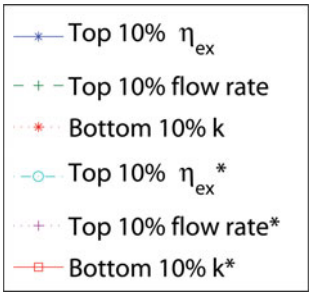


Figure 4 Legend for Figures 5 to 15. The trend lines with an asterisk describe the cases where the displacer and power cylinder are coiled.

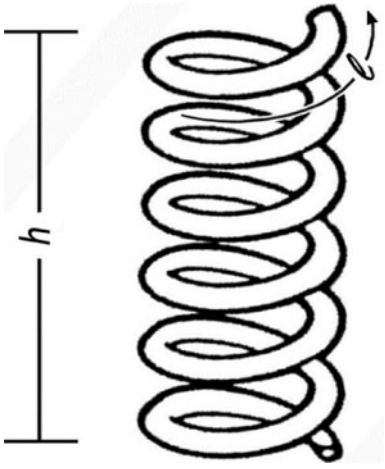


Figure 3 Coiled tube design showing the decoupling between the vertical height h and the total length l.

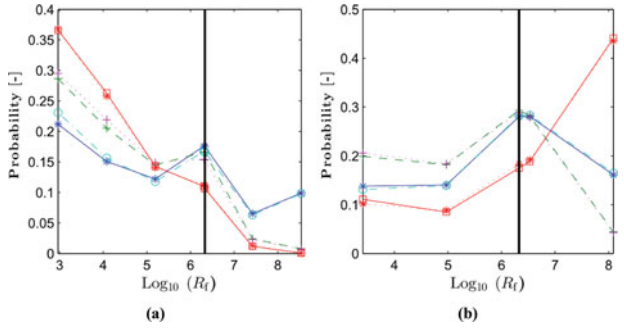


Figure 5 Number of configurations for various criteria (top 10% exergy efficiency η_{ex}, top 10% pumped flow rate, or bottom 10% gain k) depending on the resistance in the feedback connection R_f for the (a) LTP model and (b) DHX model. The black vertical line represents the nominal value of R_f.

Downloaded by [Imperial College London Library] at 09:18 20 April 2015

Table 7 Absolute values that define the bottom 10% of feedback gains k, the top 10% of pumped flow rates per unit heat input, and the top 10% of exergy efficiencies η_{ex}

	LTP			DHX		
	k	Flow rate ($f \times \eta_{ex}$)	η_{ex}	k	Flow rate ($f \times \eta_{ex}$)	η_{ex}
Regular cylinder	0.0154–5.0453	0.1363–98.54	0.4679–0.9998	0.0019–0.9226	0.0165–4.7295	0.8317–0.9979
Coiled displacer and power cylinder	0.0154–6.2311	0.1537–98.54	0.5249–0.9998	0.0019– 0.9016	0.0159–4.7295	0.8353–0.9979

Note: For a given application the flow rate per unit heat input is proportional to the product of the frequency and the exergy efficiency, $U \propto f \times \eta_{ex}$.

Sensitivity Analysis

To calculate how sensitive the three main performance indicators of the NIFTE device—namely, efficiency, flow rate, and gain—are to perturbations of the independent parameters that define the design of the device, the derivatives of the three performance indicators with respect to the device parameters are computed (e.g., $\partial\eta_{ex}/\partial R_f$, $\partial(f_0\eta_{ex})/\partial C_d$, or $\partial k/\partial L_p$). As this is computationally intensive, the load parameters L_l and R_l are set to constant values, specifically, the maximum value in the respective ranges representing the maximum load to which the device would be required to deliver in a particular practical application. The maximum load values also yield the highest exergy efficiencies. Decreasing the number of variables in this manner reduces computing time and memory usage considerably.

The sensitivity derivatives are evaluated over the entire independent parameter space, yet only the values of the derivatives that are found within the space of high efficiencies, high flow rates, or low gains are considered. This is because high sensitivities in otherwise poorly performing device configurations were not considered interesting cases to analyze.

RESULTS AND DISCUSSION

Figure 4 presents the legend used in Figures 5 through 15, which show results associated with NIFTE device configurations that attain: (i) the highest 10% exergy efficiencies η_{ex}; (ii) the highest 10% pumped volumetric flow rates per unit heat input; or (iii) the lowest 10% feedback gains k (related to the temperature difference imposed across the device heat exchangers in the LTP, and the heat input to the device heat exchangers in the DHX). Specifically, having identified all NIFTE configurations for which the device will attain this desired performance, these figures show the probability functions of each one of the 11 investigated independent R, L or C parameters within this subset of configurations. Each particular NIFTE configuration/design is associated with a given set of RLC parameter values. Thus, the functions shown in these figures indicate the probability that an RLC parameter will take a particular value, given that the NIFTE device exhibits high efficiency, high flow rate, or low gain. Each one of these plots can thus be interpreted as indicating the value or range of values of a particular parameter (where the probability is greatest) for which the NIFTE device attains this desired performance. In the order with which they appear in Figures 5 to 15, these are R_f, R_{th}, R_l, C_p, C_d, C_{ad}, L_p, L_d, L_f, L_l, and C_{hx}. The legend that corresponds to all plots can be found in Figure 4. The asterisk denotes configurations where the displacer and power tubes are coiled. In each figure, the left-hand plots represent the parameters for the LTP model, and the right-hand plots represent the same parameters for the DHX model. The absolute values of the highest 10% of efficiencies and flow rates as well as the lowest 10% of gains, are listed in Table 7. Note that the values in the second and the fourth columns are not absolute values of the flow rate, but instead, the product of the exergy efficiency and oscillation frequency. The pumped volumetric flow rate per unit heat input is proportional to this product: $U \propto f \times \eta_{ex}$. Furthermore, Table 8 lists the values of each parameter that resulted in the highest number of occurrences for the exergy efficiencies, the flow rates, and the feedback gains listed in Table 7.

Table 8 Best values of the LTP and DHX model parameters for different optimization conditions

	Efficiency optimization		Flow rate optimization		Feedback gain optimization		
Electrical element	LTP	DHX	LTP	DHX	LTP	DHX	Units
R_{th}	3.13×10^{7}	3.13×10^{7}	3.13×10^{7}	7.20×10^{9}	3.13×10^{7}	3.13×10^{7}	kg/m^4-s
R_l	4.07×10^{7}	1.51×10^{10}	4.07×10^{7}	4.07×10^{7}	4.08×10^{0}	1.51×10^{10}	kg/m^4-s
R_f	9.23×10^{2}	3.38×10^{6}	9.23×10^{2}	2.13×10^{6}	9.23×10^{2}	1.22×10^{8}	kg/m^4 -s
C_{ad}	9.84×10^{-11}	9.84×10^{-11}	9.84×10^{-11}	9.84×10^{-11}	1.40×10^{-7}	1.40×10^{-7}	m^4-s^2/kg
C_p	5.48×10^{-7}	1.29×10^{-6}	7.58×10^{-9}	1.17×10^{-7}	9.89×10^{-7}	3.89×10^{-7}	m^4-s^2/kg
C_d	1.80×10^{-7}	2.05×10^{-7}	1.80×10^{-7}	2.05×10^{-7}	2.71×10^{-8}	2.05×10^{-7}	m^4-s^2/kg
C_{hx}	—	3.82×10^{-6}	—	3.25×10^{-10}	—	3.82×10^{-6}	m^4-s^2/kg
L_l	1.27×10^{8}	4.24×10^{9}	1.27×10^{8}	1.27×10^{8}	1.27×10^{3}	4.24×10^{9}	kg/m^4
L_p	9.04×10^{5}	1.15×10^{6}	9.04×10^{5}	1.15×10^{6}	2.76×10^{5}	1.15×10^{6}	kg/m^4
L_f	6.68×10^{4}	6.86×10^{6}	6.68×10^{4}	4.74×10^{6}	6.68×10^{4}	5.21×10^{7}	kg/m^4
L_d	1.03×10^{6}	1.83×10^{6}	2.68×10^{6}	1.83×10^{6}	7.01×10^{6}	1.83×10^{6}	kg/m^4

Downloaded by [Imperial College London Library] at 09:18 20 April 2015

Downloaded by [Imperial College London Library] at 09:18 20 April 2015

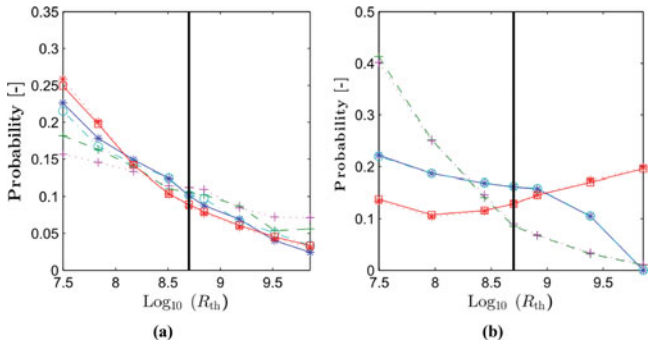


Figure 6 Number of configurations for various criteria (top 10% exergy efficiency η_{ex}, top 10% pumped flow rate, or bottom 10% gain k) depending on the thermal resistance R_{th} for the (a) LTP model and (b) DHX model. The black vertical line represents the nominal value of R_{th}.

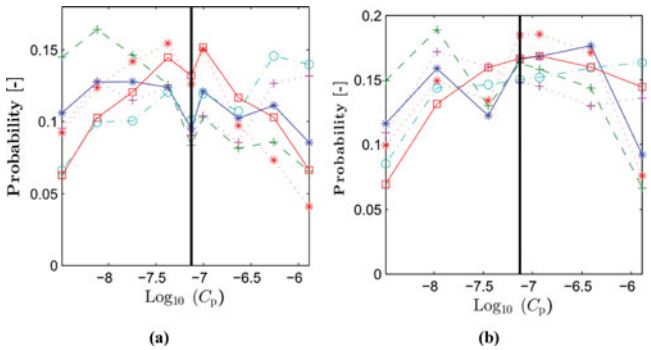


Figure 8 Number of configurations for various criteria (top 10% exergy efficiency η_{ex}, top 10% pumped flow rate, or bottom 10% gain k) depending on the capacitance of the power cylinder C_p for the (a) LTP model and (b) DHX model. The black vertical line represents the nominal value of C_p.

A first observation is that the highest calculated NIFTE efficiencies as estimated from the models herein tend to be similar or higher compared to other low-grade heat conversion systems. Schuster et al. [19] performed an efficiency optimization for sub- and supercritical organic Rankine cycles (ORCs) for different working fluids. Exergy efficiencies as high as 80% for subcritical and supercritical cycles and 90% for supercritical cycles were obtained for a heat source temperature of 210°C, a heat sink at ambient conditions, and with isopentane as the working fluid. Wang et al. [20] designed a cogeneration cycle, consisting of an ORC and an adsorption refrigeration cycle as first- and second-stage cycle, driven by solar heat at lower than 100°C. The authors reported an exergy efficiency from 84% to 89%. Chen et al. [21], on the other hand, considered a transcritical Rankine cycle with CO_2 and R32 as working fluids. The heat source temperature here was 180°C, and again, the heat sink was at ambient temperature. This model predicted maximum exergy efficiencies at 50% for CO_2 and 60% for R32. Madhawa Hettiarachchi et al. [22] modeled a geothermal organic Rankine cycle running on the same working fluid as the NIFTE, namely, *n*-pentane. A comparably low maximum exergy efficiency of 16% was reported here due to the low heat source temperature of just 90°C and a fairly high heat sink temperature of 30°C. Other references calculated maximum exergy efficiencies between 45% and 60% for a variety of working fluids, such as hydrocarbons, refrigerants, or inorganic substances, and heat source temperatures ranging from 145°C to 200°C [3, 23]. In summary, our estimated efficiencies for the NIFTE and those in the literature for other cycles are in reasonable agreement, especially given that the present LTP and DHX models of NIFTE do not include a loss parameter to account for thermodynamic losses due to parasitic heat transfer (condensation) [8], which would lead to lower predicted exergy efficiency values than what has been obtained here.

Optimizing for Higher Efficiencies

Efficiency holds the utmost importance in the design of any heat engine. Optimizing the NIFTE for higher exergy efficiencies requires finding the subset of best combinations of RLC component values that allow the device to exhibit the highest (e.g., top 10%) efficiencies out of the 3.5 million (for the LTP model with noncoiled cylinders) geometrically realistic parameter combinations tested. The number of occurrences of each parameter value can then be found within this high-efficiency NIFTE subset, and the values of the various parameters with the greatest occurrence can be identified.

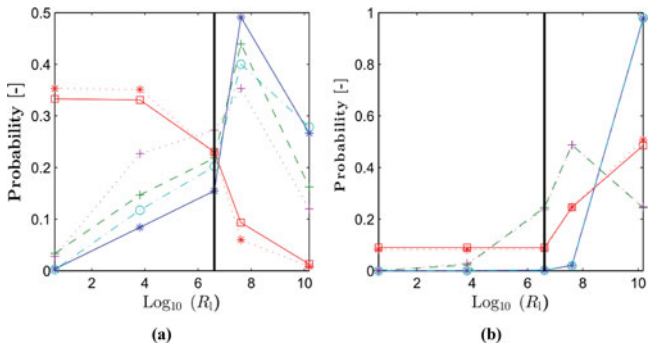


Figure 7 Number of configurations for various criteria (top 10% exergy efficiency η_{ex}, top 10% pumped flow rate, or bottom 10% gain k) depending on the resistance in load line R_l for the (a) LTP model and (b) DHX model. The black vertical line represents the nominal value of R_l.

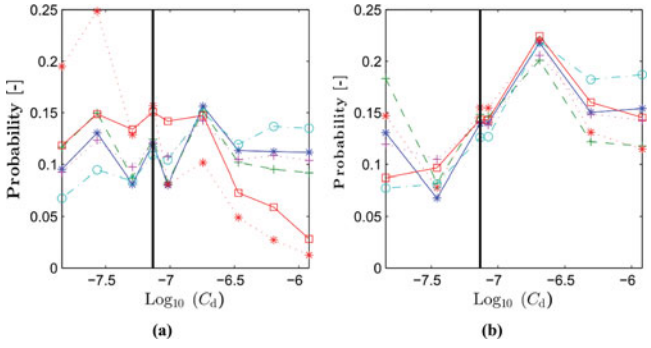


Figure 9 Number of configurations for various criteria (top 10% exergy efficiency η_{ex}, top 10% pumped flow rate, or bottom 10% gain k) depending on the capacitance of the displacer cylinder C_d for the (a) LTP model and (b) DHX model. The black vertical line represents the nominal value of C_d.

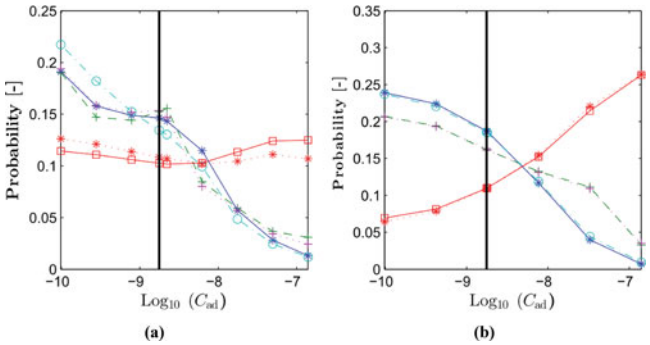


Figure 10 Number of configurations for various criteria (top 10% exergy efficiency η_{ex}, top 10% pumped flow rate, or bottom 10% gain k) depending on the capacitance of the adiabatic vapor volume C_{ad} for the (a) LTP model and (b) DHX model. The black vertical line represents the nominal value of C_{ad}.

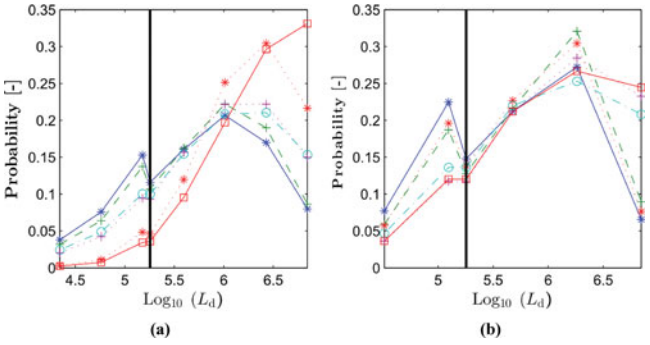


Figure 12 Number of configurations for various criteria (top 10% exergy efficiency η_{ex}, top 10% pumped flow rate, or bottom 10% gain k) depending on the inductance of the displacer cylinder L_d for the (a) LTP model and (b) DHX model. The black vertical line represents the nominal value of L_d.

Downloaded by [Imperial College London Library] at 09:18 20 April 2015

Figures 5 and 6 show that LTP model configurations that exhibit high exergy efficiencies tend to have small fluid flow resistances in the feedback connection R_f and small thermal resistances in the heat exchangers R_{th}. This was also the conclusion reached in several previous efforts [5, 6, 9], and can be understood in terms of the reduced dissipation in the respective dissipative components. The DHX model results in Figures 5 and 6 are similar in terms of the role of the thermal resistance R_{th}, but indicate that an intermediate value of feedback resistance R_f close to the nominal value has the greatest probability of being associated with high-efficiency NIFTE designs. This may seem at first glance to contradict the findings already stated. However, it has been observed in reference [7] that for (otherwise) nominal configurations pumping into a low load resistance, higher efficiencies are attained at low feedback resistances, while for nominal configurations pumping into a high load resistance R_l, higher efficiencies are attained at high feedback resistances. It must be noted that in our study all parameters were varied simultaneously (and not one at a time), and we are regarding the parameter combinations with the highest efficiencies over the entire parameter space. In reference [7], only nominal cases with low and high R_l were compared.

Generally, the top 10% most efficient device configurations appear in relation to applications with load resistances R_l higher than nominal, as indicated in Figure 7. This is especially the case for the DHX model. This is to be expected, as the exergy efficiency is defined as the power dissipated in the load over the total exergy input to the system, and a high load resistance will lead to proportionally higher dissipation in this component for a given flow rate. Similarly, a relatively high load inductance L_l also gives rise to configurations with higher efficiencies (see Figure 14, shown later). These findings are in direct agreement with those in previous parametric studies [5–7, 9]. However, it should be noted that R_l and L_l are not perturbed independently of each other but are always changed together. This explains the almost identical behavior of all performance values with regards to the two parameters.

The results in Figure 13 (shown later) suggest that, in a fashion similar to the feedback connection resistance R_f, the feedback tube inductance L_f is typically low (for the LTP model) or around the nominal value (for the DHX model) when high efficiencies are attained. Furthermore, the high-efficiency values of the inductances in the power and displacer cylinders, L_p and L_d, are plotted in Figures 11 and 12 (shown later), respectively. The inductances for high-efficiency are found to have values around nominal for L_p and values an order of magnitude greater than nominal for L_d. Likewise, Markides and Smith [5] reported that at nominal conditions higher

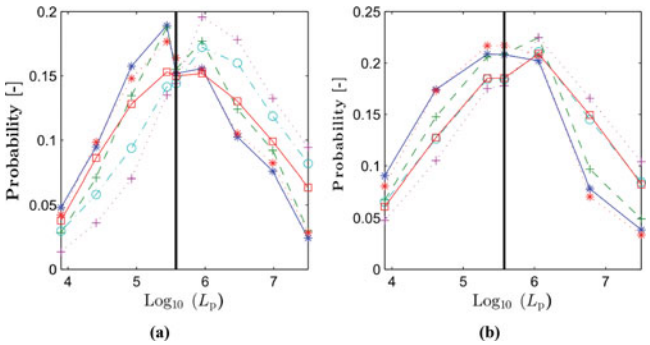


Figure 11 Number of configurations for various criteria (top 10% exergy efficiency η_{ex}, top 10% pumped flow rate, or bottom 10% gain k) depending on the inductance of the power cylinder L_p for the (a) LTP model and (b) DHX model. The black vertical line represents the nominal value of L_p.

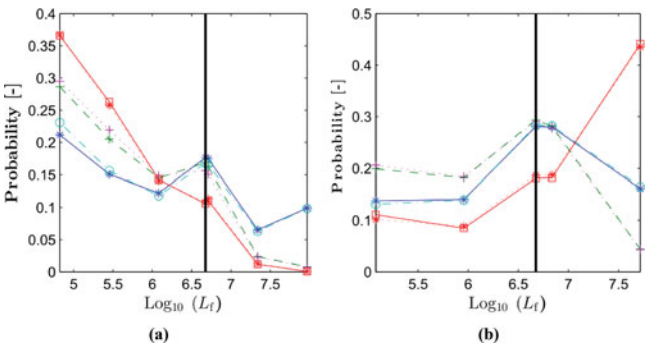


Figure 13 Number of configurations for various criteria (top 10% exergy efficiency η_{ex}, top 10% pumped flow rate, or bottom 10% gain k) depending on the inductance of the feedback tube L_f for the (a) LTP model and (b) DHX model. The black vertical line represents the nominal value of L_f.

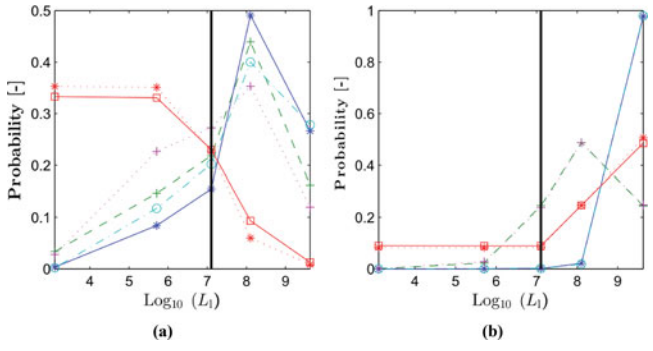


Figure 14 Number of configurations for various criteria (top 10% exergy efficiency η_{ex}, top 10% pumped flow rate, or bottom 10% gain k) depending on the inductance of the load line L_l for the (a) LTP model and (b) DHX model. The black vertical line represents the nominal value of L_l.

inductances of the power and displacer cylinders yield better efficiencies.

The trends pertaining to the power and displacer cylinder capacitances C_p (Figure 8) and C_d (Figure 9) are not as clear (or strong) as for the various resistances and inductors in the device. Both capacitances ought to be reasonably high especially with coiled designs; that is, one requires a low capacity of the power and the displacer cylinders to store/release potential (hydrostatic) energy per unit flow rate for higher efficiencies. More specifically, coiled designs should have C_p values at or slightly below the maximum investigated value in these results. For noncoiled designs, the LTP model predicts high efficiencies at C_p values about one order of magnitude below the nominal value, while the DHX model predicts high efficiencies at an order of magnitude above the nominal value. For the capacitance in the displacer cylinder C_d, the optimal value for both models is about one order of magnitude above the nominal value. Either way, the sensitivity to the value of these parameters for high efficiency is reduced compared to some of the parameters commented on previously (e.g., R_l, R_{th}). Markides

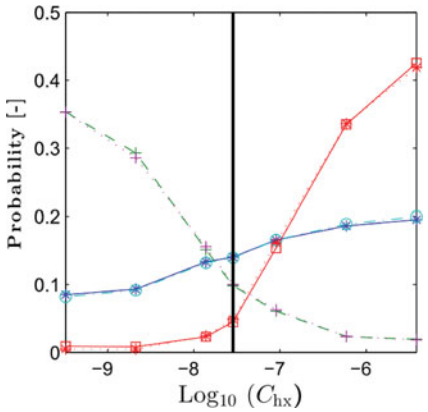


Figure 15 Number of configurations for various criteria (top 10% exergy efficiency η_{ex}, top 10% pumped flow rate, or bottom 10% gain k) depending on the heat exchanger storage capacitance C_{hx} for the DHX model. The black vertical line represents the nominal value of C_{hx}.

and Smith [5] reported that low C_p values can be beneficial for nominal configurations, while C_d had little influence on the efficiency. The same study also found that the capacitance of the adiabatic vapor volume C_{ad} is high at high exergy efficiencies for nominal configurations. Contrary to this observation, the optimal configurations investigated here have low adiabatic vapor volume capacitances (see Figure 10).

The results from the DHX model are mainly similar to those made with the LTP model. In addition, higher heat exchanger capacitances C_{hx} tend to allow higher efficiencies, although the sensitivity to this parameter as revealed later in this work is not high. Both observations do not follow from the findings made in the parametric study in reference [9], highlighting the importance of performing the present multiparametric optimization analysis. The agreement in the findings concerning the role of the parameters in the LTP and DHX models is nontrivial and favorable for the further development of the NIFTE technology, as it indicates that the conclusions hold independently of the model chosen to represent the device. It is noted that it is arguable which model is a better representation of the NIFTE prototype. It would be expected, in fact, that each model will be the preferred representation of this device in different operation regimes.

Table 8 summarizes the parameter values which occur with the greatest frequency within the high efficiency NIFTE configuration subset. In addition, Table 9 lists the geometrical dimensions of NIFTE components corresponding to the specific parameter configuration that results in the highest absolute value for exergy efficiency.

Optimizing for Higher Normalized Pumped Volumetric Flow Rates

High pumped flow rates are also a desirable feature, given that the technology is envisaged primarily as a fluid pumping device. It is important to emphasize that a higher frequency is not sufficient for a high flow rate. The flow rate per unit heat input is directly proportional to the product of exergy efficiency (η_{ex}) and the operational frequency (f_0) of the device. Here, the study focuses on the NIFTE configurations that exhibit the highest 10% of flow rates from all 3.5 million (or 4 million for DHX) tested configurations.

Figures 5, 6, and 10 indicate that the feedback connection and thermal resistances R_f and R_{th}, and the adiabatic vapor volume capacitance C_{ad}, all tend to be small for high flow rates. An exception can be seen for the feedback resistance R_f in the DHX model, which exhibits high flow rates at nominal feedback resistances, similar to what was observed with regards to the exergy efficiency. The close link between the conclusions regarding the exergy efficiency and those regarding the pumped volumetric flow rate (recall that $U \propto f \times \eta_{ex}$) suggests that the changes made to the efficiency are significantly larger than those made to the operational frequency of this device when these parameter values are perturbed, such that the multiple of these two is determined by the changes to the former. The

Downloaded by [Imperial College London Library] at 09:18 20 April 2015

Table 9 Geometrical values for the most efficient configuration, the configuration with the highest flow rate, and the configuration with the lowest feedback gain

	Most efficient configuration		Configuration with highest flow rate		Configuration with lowest gain		
Dimension	LTP	DHX	LTP	DHX	LTP	DHX	Units
d_d	0.025	0.1	0.02	0.025	0.025	0.06	m
d_f	0.029	0.023	0.029	0.002	0.029	0.002	m
d_l	0.05	0.003	0.1	0.01	0.1	0.003	m
d_p	0.1	0.1	0.1	0.1	0.043	0.055	m
l_d	1	5.607	0.273	2.587	1	12.4	m
l_f	0.069	0.078	0.069	0.314	0.069	0.314	m
l_l	0.992	30	0.01	1	0.01	30	m
l_p	1.069	14.5	0.327	2.76	0.861	0.03	m
V_{eq}	1.09×10^{-5}	1.09×10^{-5}	1.09×10^{-5}	1.94×10^{-5}	0.0154	0.0154	m^3

Downloaded by [Imperial College London Library] at 09:18 20 April 2015

results in Figures 8 and 9 for the power and displacer cylinder capacitances, C_p and C_d, do not show clear trends.

When considering the high flow rate results with respect to the power cylinder and displacer cylinder inductances in Figures 11 (for L_p) and 12 (for L_d), the high flow rate NIFTE configurations show peaks that occur at their respective nominal values or at higher values, as with the efficiency results discussed previously. In addition, for the feedback tube inductance L_f depicted in Figure 13, high flow rates tend to occur for low values in the LTP model, while for the DHX L_f behaves similarly to the other two inductances.

As before with the exergy efficiency, the results and trends from the DHX model do not differ considerably from the LTP. In addition, high flow rates are associated with small heat exchanger capacitance C_{hx} values. Interestingly, this is not the same conclusion as that reached for the efficiency, which indicates that the heat exchanger capacitance C_{hx} has a strong effect on the oscillation frequency. The observed lower flow rates when the capacitance is higher suggest that high values slow the operation of the NIFTE. The best values of the components for higher flow rates are summarized in Table 8. Table 9 lists the geometrical dimensions of the configuration that yielded the highest flow rate.

Finally, for the load parameters, R_l and L_l (Figures 7 and 14), high flow rates are associated with values about one order of magnitude greater than the selected nominal values, but not higher. This conclusion holds for both coiled and noncoiled designs, and arises from the results of both the LTP and the DHX models.

Optimizing for Lower Feedback Gains

From the earlier methodology section describing the heat exchange models in the thermal domain, we know that the feedback gain k in the LTP model is proportional to the temperature gradient on the heat exchanger walls dT_{hx}/dy, and proportional to the power gradient in the heat exchanger blocks $d\dot{Q}_{hx}/dy$ in the DHX model. An optimization of the NIFTE should require the pump to be designed for a lower temperature difference or lower power gradient in the heat exchangers, which indirectly corresponds to the lowering of the power consumption for operating the pump and to the ability to convert lower grade heat. Therefore, the characteristics of the RLC component values in the NIFTE device configurations associated with the lowest 10% of feedback gain values among the 3.5 million (or 4 million) tested NIFTE combinations were also investigated.

Figures 5 to 7 show that for the LTP model, low resistance values (R_f, R_{th}, and R_l) allow lower feedback gain values. This has also been confirmed for parametric studies based on nominal configurations, where low feedback and load line resistances R_f and R_l facilitate smaller feedback gains [6, 7, 9]. For the DHX model, however, there is a different trend whereby high resistances with the DHX correlate, to some extent although not strongly, with lower gain values in this case, something that has not been observed previously. It is also noted that Solanki et al. [7], who investigated parametrically the effect of varying R_f in the DHX model with otherwise nominal parameters, reported that lower values for the feedback resistance resulted in lower gains. Again, this demonstrates the importance of performing a multi-parametric analysis over the entire design space, rather than simple one-parameter perturbations from the nominal design, which may itself be far from an ideal configuration.

The capacitances do not all behave in a similar way, as is the case with resistances. For the LTP model, intermediate power and displacer cylinder capacitances C_p and C_d, around or below their nominal values, were beneficial with regards to gain, as can be inferred from Figures 8 and 9. For coiled designs the low-gain LTP configurations have low values of C_d. Markides et al. [9] reported that a small value for C_p produced low gains for a nominal LTP device. Interestingly, as depicted in Figure 10, the capacitance of the vapor volume C_{ad} is not strongly correlated with low-gain NIFTE designs with the LTP model. For the DHX model, nominal values for C_p (Figure 8) and reasonably high values for C_d and C_{ad} (Figures 9 and 10) are beneficial, especially for the latter. In addition, Figure 15 shows that low gains arise for high values of the heat exchanger capacitance C_{hx}, with this parameter being a strong determining factor in the NIFTE DHX model attaining low gains.

Table 10 Normalized gradients (with respect to the corresponding nominal values of each parameter) from the sensitivity analysis: maximum absolute values of derivatives over the ranges that exhibit optimal system performance, with coiling

	Efficiency $\frac{\partial \eta_{ex}}{\partial x} \times \tilde{x}$		Flow rate $\frac{\partial (f_0.\eta_{ex})}{\partial x} \times \tilde{x}$		Feedback gain $\frac{\partial k}{\partial x} \times \tilde{x}$	
x	LTP	DHX	LTP	DHX	LTP	DHX
R_{th}	1.05×10^{5}	7.23×10^{3}	1.22×10^{5}	4.60×10^{3}	9.55×10^{10}	2.63×10^{4}
R_f	1.45×10^{-2}	8.69×10^{-5}	1.01×10^{-2}	3.99×10^{-4}	1.75×10^{2}	8.31×10^{-4}
C_{ad}	4.94×10^{0}	2.27×10^{-1}	4.38×10^{0}	3.48×10^{-1}	2.06×10^{6}	2.14×10^{-1}
C_p	1.61×10^{1}	6.71×10^{-2}	1.03×10^{1}	2.67×10^{-1}	5.44×10^{7}	3.59×10^{3}
C_d	4.35×10^{0}	2.24×10^{-2}	2.19×10^{0}	8.41×10^{-2}	1.26×10^{7}	3.05×10^{-1}
L_p	4.62×10^{0}	3.57×10^{-2}	1.26×10^{1}	1.80×10^{-3}	1.22×10^{8}	3.13×10^{-7}
L_f	1.74×10^{1}	2.74×10^{-3}	1.03×10^{1}	2.38×10^{-2}	1.53×10^{8}	4.40×10^{-6}
L_d	3.61×10^{0}	1.08×10^{-4}	1.67×10^{0}	8.43×10^{-4}	1.27×10^{7}	1.75×10^{-7}
C_{hx}	—	1.26×10^{-1}	—	1.05×10^{0}	—	3.39×10^{0}

For the inductances, a close to nominal power cylinder inductance L_p (Figure 11) and a high displacer cylinder inductance L_d (Figure 12) lead to low-gain configurations, irrespective of the NIFTE model chosen. On the other hand, the two models show opposite results when considering the feedback and load line inductances. Specifically, the LTP model suggests the use of low L_f and L_l, whereas the DHX model suggests high L_f and L_l. When using the LTP model, Solanki et al. [6] and Markides et al. [9] both found the optimal load line inductance L_l to be slightly above its nominal value. In addition, reference [7] reported low gains at the higher end of values of L_f for nominal configurations with the DHX model.

Optimal Design Overview

In summary to the findings that were identified and discussed in the previous sections, the LTP model suggests that a highly efficient NIFTE will tend to require minimal thermal R_{th} and feedback tube R_f resistances, as well as minimal feedback tube inductances L_f and adiabatic volume capacitances C_{ad}. All other parameters can be either around their respective nominal values (e.g., L_f, L_p), or above these values by one order of magnitude, but not higher (e.g., R_l, L_d). The power and displacer cylinder capacitances in the LTP model do not have a strong role to play in determining the exergy efficiency of the NIFTE device. The DHX model predictions are similar, except for the feedback tube resistance R_f, which should be nominal, while the load resistance R_l, the inductance L_l, and the heat exchanger capacitance C_{hx} should be as high as possible. There is also an indication from the DHX model that displacer capacitance should be about 3 times higher than nominal.

To maximize flow rate, the LTP model indicates that the values of the resistances R_{th} and R_f, the capacitance C_{ad}, and the inductance L_f should be as low as possible while all other parameters should be nominal or above nominal, in line with the observations concerning the exergy efficiency. Unlike the previous findings for the efficiency, both LTP and DHX models agree that a load with a high resistance R_l and inductance L_l, in both cases by one order of magnitude relative to their respective nominal values, will tend to allow for high flow rates. The DHX model only differs in that it predicts the optimal feedback tube parameters R_f and L_f to be nominal, while the heat exchanger capacitance C_{hx} should be minimal.

The LTP and DHX model diverge significantly with regard to the feedback gain k required for oscillatory operation. While the DHX model predicts reasonably high (near or above nominal) or maximum values for almost all parameters, the LTP model predicts minimal or low values for the same parameters. The few parameters in which both models coincide are the power cylinder parameters C_p and L_p (both nominal) and the displacer cylinder parameters C_d (nominal) and L_d (high).

Table 11 Normalized gradients (with respect to corresponding nominal values of each parameter) from the sensitivity analysis: mean absolute values of derivatives over the ranges that exhibit optimal system performance, with coiling

	Efficiency, $\frac{\partial \eta_{ex}}{\partial x} \times \tilde{x}$		Flow rate, $\frac{\partial (f_0.\eta_{ex})}{\partial x} \times \tilde{x}$		Feedback gain, $\frac{\partial k}{\partial x} \times \tilde{x}$	
x	LTP	DHX	LTP	DHX	LTP	DHX
R_{th}	8.68×10^{3}	1.13×10^{3}	5.86×10^{3}	3.18×10^{2}	1.19×10^{8}	1.25×10^{2}
R_f	2.04×10^{-4}	2.72×10^{-6}	2.35×10^{-4}	2.08×10^{-5}	1.34×10^{1}	3.10×10^{-5}
C_{ad}	1.49×10^{0}	1.09×10^{-2}	8.45×10^{-1}	7.32×10^{-2}	5.72×10^{3}	6.10×10^{-3}
C_p	1.70×10^{-2}	5.51×10^{-4}	2.08×10^{-1}	6.60×10^{-3}	2.49×10^{4}	9.51×10^{-3}
C_d	5.29×10^{-2}	3.81×10^{-4}	3.32×10^{-2}	1.90×10^{-3}	6.12×10^{3}	6.80×10^{-3}
L_p	3.96×10^{-3}	1.78×10^{-5}	1.49×10^{-2}	1.11×10^{-5}	1.92×10^{4}	6.47×10^{-9}
L_f	9.66×10^{-2}	3.50×10^{-6}	9.25×10^{-2}	1.48×10^{-4}	2.67×10^{4}	4.66×10^{-7}
L_d	4.30×10^{-3}	1.36×10^{-7}	4.50×10^{-3}	5.51×10^{-6}	2.77×10^{3}	1.77×10^{-8}
C_{hx}	—	3.00×10^{-3}	—	2.52×10^{-1}	—	7.70×10^{-3}

Downloaded by [Imperial College London Library] at 09:18 20 April 2015

Downloaded by [Imperial College London Library] at 09:18 20 April 2015

Sensitivity Analysis Results

Tables 10 and 11 list the maximum and mean values of the derivatives of the exergy efficiencies, pumped flow rates and feedback gains with respect to all NIFTE parameters apart from R_l and L_l, which were set to their highest respective values. The latter two parameters were not varied, as this would have been computationally too intensive. The derivatives were calculated over the whole space of possible NIFTE configurations, including also those that are geometrically impossible. However, for the maximum and mean values, solely the subset corresponding to the top 10% in efficiency or flow rate, or bottom 10% in feedback gain, were considered. It is observed, from Table 10, that the maximum sensitivity values can be very high; this is due to the existence of local discontinuities in the results considered here, which were also reported in earlier work (e.g., [7]). Furthermore, one can see that the DHX model has, generally, lower maximum values, which correlates with the finding in reference [7] that this model was less susceptible to discontinuities than the LTP owing to the existence of the additional heat exchanger capacitance C_{hx}. Therefore, although the high maximum sensitivity values are not incorrect, this observation suggests that the mean sensitivities over the range of the parameter space associated with high-performance NIFTE configurations (Table 11) may be a more reliable and consistent indicator from which more general conclusions can be drawn.

As a general rule, the mean derivatives in Table 11 are, as before, higher for the LTP model than for the DHX. Hence, it is possible to conclude that the presence of the heat exchanger thermal storage capacitance C_{hx} acts to reduce the overall sensitivity of the model. All three optimization parameters (efficiency, flow rate, and feedback gain) appear least sensitive to the inductances. The results from both models indicate that the thermal resistance in the heat exchangers R_{th} is the parameter that exhibits the highest sensitivities with respect to efficiency and flow rate, followed by the compressibility of the adiabatic volume C_{ad} and the hydrostatic capacitance of the power cylinder C_p. Similarly, the feedback gain k is highly sensitive to the thermal resistance R_{th}. However, the two models differ in their sensitivities to the other parameters. For the LTP model, the highest sensitivities, following those associated with the thermal resistance, are observed for the inductances. On the other hand, the sensitivities toward the inductances are negligible in the DHX model and it is the capacitances that exhibit a much higher sensitivity. Generally, the sensitivity values of k in the LTP are extremely high compared to the values of the other parameters. Conversely, the sensitivity values of k in the DHX model are the lowest of all sensitivity values.

CONCLUSIONS

This paper presents results from the first multiparametric study reported in the literature that was conducted on the NIFTE LTP and DHX models [4–9], which have been validated against an early-stage experimental NIFTE water-pump prototype [4, 11, 12]. All system parameters (specifically the electrical resistor, inductor, and capacitor components that describe the dynamic processes undertaken in the system) were perturbed simultaneously and independently in ranges similar to those from references [5–9]. Care was taken to exclude parameter combinations that resulted in improbable or impossible geometrical combinations. From the 200 million possible combinations that correspond to a range of geometrical and fluid characteristics, the geometrically unrealistic combinations were excluded and subsets of configurations exhibiting the highest efficiencies (top 10% of cases), highest pumped flow rates per unit heat input (top 10% of cases), and lowest feedback gains (bottom 10% of cases) were examined more closely to reveal how these correlate with the values of the independent parameters. Since long displacer and power cylinders increase efficiency, spiral tubes were taken into consideration; the advantage of this design is that the length of the cylinder can be increased while not detrimentally increasing the overall dimension/size of the device.

It is concluded for the NIFTE device that, as a general rule, configurations that maximize efficiency and flow rate tend to have thermal resistances and adiabatic vapor volume capacitances that are lower than the employed nominal values in this work, which were taken as representative of the NIFTE water-pump prototype [4–9, 11, 12]. In addition, the feedback tube resistance and inductance should be around nominal or lower than this (the two models diverge slightly on this point), the displacer cylinder and load parameters should be somewhat higher than nominal, and the inductance of the power cylinder has its optimum at the selected nominal value. The effect of the heat exchanger thermal storage parameter, through the associated capacitance, on the performance of the DHX model was also investigated. Both this capacitance and the other remaining parameter, the power cylinder capacitance, must be high for optimal efficiencies but low for optimal flow rates, although in general, the power and displacer cylinder capacitances do not strongly affect the investigated performance indicators of the NIFTE device. A clear conclusion concerning the minimization of the feedback gain has proven difficult to determine, since the LTP and DHX models deliver contradictory results. The DHX model predicted that all parameters must be high with the exception of the power cylinder variables, which were near-optimal at nominal values. The LTP model, on the other hand, predicted that all parameters should be low for low gains, with the exception of, again, the power cylinder parameters (which should be nominal) and the displacer inductance (which should be high).

The interesting discrepancies between the indications concerning the LTP and DHX models of the NIFTE arise due to the presence of the heat exchanger capacitance and the nature of the dynamic heat source and sink, mostly with respect to the effects of the inductances and to some extent the capacitances (and in particular in the displacer cylinder). The DHX can be considered a slightly more realistic model when compared to the reported NIFTE prototype [8], so the optimal parameter values from the DHX part of this present study can be taken as useful

indications toward an improved design for a prototype NIFTE.

Finally, the performance sensitivity values were found to be generally higher in the LTP model than the DHX model, which is an indication that the DHX model is less susceptible to discontinuities due to the existence of the heat exchanger capacitance. This finding is in excellent agreement with direct indications of this behavior from previous work [7]. Generally, the performance of the NIFTE was least sensitive to the inductances, especially for the efficiency and flow rate. The highest sensitivities were observed for the thermal resistance in the heat exchangers, followed by the capacitances of the vapor volume, heat exchanger block, and power cylinder. In summary, among all NIFTE components beyond the load, the heat exchangers, adiabatic vapor volume, and power cylinder have the strongest influence on the performance parameters (efficiency, flow rate, feedback gain).

Downloaded by [Imperial College London Library] at 09:18 20 April 2015

NOMENCLATURE

A	cross-sectional area, m^2
C	capacitance, m^4-s^2/kg
CHX	cold heat exchanger
$C(s)$	dimensionless closed-loop transfer function
d	diameter, m
DHX	dynamic heat exchanger
E	voltage, V
f_0	marginal stability oscillation frequency, 1/s
F	resultant force on liquid in pipe, N
g	acceleration due to gravity, m/s^2
$G(s)$	dimensionless forward transfer function
h	convective heat transfer coefficient, W/m^2-K
h_d	height of coiled displacer cylinder, m
HHX	hot heat exchanger
h_p	height of coiled power cylinder, m
I	current, A
k	feedback gain (k, k_{LTP}: dimensionless; k_{DHX}: 1/s)
l	length, m
L	inductance, kg/m^4
LTP	linear temperature profile
m	mass, kg
NIFTE	non-inertive-feedback thermofluidic engine
P	pressure, Pa
ΔP	pressure difference, Pa
$\dot{Q}$	heat flow rate, W
R	resistance, kg/m^4-s
s	Laplace domain variable, 1/s
Δs_{fg}	specific entropy change for vaporization, J/kg-K
S	surface area of heat exchanger blocks, m^2
$\dot{S}$	rate of entropy generation, entropy flow rate, W/K
t	time, s
T	temperature, K
U	volumetric flow rate, m^3/s
V	volume, m^3
y	displacement in the vertical direction as per Figure 1b, m
Z	impedance, kg/m^4-s
Z_{TOT}	total impedance, kg/m^4-s

Greek Symbols

$\alpha_i, \beta_i, \gamma_i$	transfer functions in NIFTE model i, where i = LTP or DHX
γ	ratio of specific heat capacities of the working fluid in the vapor phase
η_{ex}	exergy efficiency
ρ	density, kg/m^3
μ	dynamic (absolute) viscosity, kg/m-s

Subscripts

ad	adiabatic vapor volume
d	displacer cylinder
f	feedback connection/line
hx	heat exchanger
l	load line
wf	working fluid
p	power cylinder
pen	pentane
w	water
th	thermal

Superscript

*	values corresponding to a coiled displacer or power cylinder design

REFERENCES

[1] Markides, C. N., The Role of Pumped and Waste Heat Technologies in a High-Efficiency Sustainable Energy Future for the UK, *Applied Thermal Energy*, vol. 53, no. 2, pp. 197–209, 2013.

[2] Crook, A. W., *Profiting From Low-Grade Heat: Thermodynamic Cycles for Low-Temperature Heat Sources*, Institution of Electrical Engineers, London, UK, 1994.

[3] Dai, Y., Wang, J., and Gao, L., Parametric Optimization and Comparative Study of Organic Rankine Cycle (ORC) for Low-Grade Heat Recovery, *Energy Conversion and Management*, vol. 50, no. 3, pp. 576–582, 2009.

[4] Smith, T. C. B., Thermally Driven Oscillations in Dynamic Applications, Ph.D. Thesis, University of Cambridge, Cambridge, UK, 2006.

[5] Markides, C. N., and Smith, T. C. B., A Dynamic Model for the Efficiency Optimization of an Oscillatory Low Grade Heat Engine, *Energy*, vol. 36, no. 12, pp. 6967–6980, 2011.

[6] Solanki, R., Galindo, A., and Markides, C. N., Dynamic Modelling of a Two-Phase Thermofluidic Oscillator for Ef-

ficient Low Grade Heat Utilization: Effect of Fluid Inertia, *Applied Energy*, vol. 89, pp. 156–163, 2012.

[7] Solanki, R., Galindo, A., and Markides, C. N., The Role of Heat Exchange on the Behaviour of an Oscillatory Two-Phase Low-Grade Heat Engine, *Applied Thermal Engineering*, vol. 53, pp. 197–209, 2013.

[8] Solanki, R., Mathie, R., Galindo, A., and Markides, C. N., Modelling of a Two-Phase Thermofluidic Oscillator for Low-Grade Heat Utilisation: Accounting for Irreversible Thermal Losses, *Applied Energy*, vol. 106, pp. 337–354, 2013.

[9] Markides, C. N., Osuolale, A., Solanki, R., and Stan, G.-B. V., Nonlinear Heat Transfer Processes in a Two-Phase Thermofluidic Oscillator, *Applied Energy*, vol. 104, pp. 958–977, 2013.

[10] Markides, C. N., and Gupta, A., Experimental Investigation of a Thermally Powered Central Heating Circulator: Pumping Characteristics, *Applied Energy*, vol. 110, pp. 132–146, 2013.

[11] Smith, T. C. B., Power Dense Thermofluidic Oscillators for High Load Applications, *Energy Conversion Engineering, IECEC 2004: Proceedings of the 2nd International Energy Conversion Engineering Conference*, Providence, RI, 2004.

[12] Smith, T. C. B., Asymmetric Heat Transfer in Vapour Cycle Liquid-Piston Engines, *Stirling Engine, ISEC 2005: Proceedings of the 12th International Stirling Engine Conference and Technology Exhibition*, Durham, UK, 2005.

[13] Stammers, C. W., The Operation of the Fluidyne Heat Engine at Low Differential Temperatures, *Journal of Sound and Vibration*, vol. 63, no. 4, pp. 507–516, 1979.

[14] Stevens, J. W., Low Capital Cost Renewable Energy Conversion With Liquid Piston Stirling Engines, *Proceedings of ASME 2010 4th International Conference on Energy Sustainability*, Phoenix, AZ, pp. 479–484, 2010.

[15] Reader, G. T., Stirling Regenerators, *Heat Transfer Engineering*, vol. 15, no. 2, pp. 19–25, 1994.

[16] Dorf, R. C., and Bishop, R. H., *Modern Control Systems*, Addison-Wesley, Boston, MA, 1997.

[17] Erek, A., and Dincer, I. A., New Approach to Energy and Exergy Analyses of Latent Heat Storage Unit, *Heat Transfer Engineering*, vol. 30, no. 6, pp. 506–515, 2009.

[18] Shukuya, M., and Hammache, A., Introduction to the Concept of Exergy for a Better Understanding of Low-Temperature-Heating and High-Temperature-Cooling Systems, VTT Reseach Notes 2158, April 2002.

[19] Schuster, A., Karellas, S., and Aumann, R., Efficiency Optimization Potential in Supercritical Organic Rankine Cycles, *Energy*, vol. 35, pp. 1033–1039, 2010.

[20] Wang, L., Roskilly, A. P., and Wang, R., Solar Powered Cascading Cogeneration Cycle with ORC and Adsorption Technology for Electricity and Refrigeration, *Heat Transfer Engineering*, vol. 35, no. 11–12, pp. 1028–1034, 2014.

[21] Chen, H., Goswami, D. Y., Rahman, M. M., and Stefanakos, E. K., Energetic and Exergetic Analysis of CO_2- and R23-Based Transcritical Rankine Cycles for Low-Grade Heat Conversion, *Applied Energy*, vol. 88, pp. 2802–2808, 2011.

[22] Madhawa Hettiarachchi, H. D., Golubovic, M., Worek, W. M., and Ikegami, Y., Optimum Design Criteria for an Organic Rankine Cycle Using Low-Temperature Geothermal Heat Sources, *Energy*, vol. 32, pp. 1698–1706, 2007.

[23] Mago, P. J., Chamra, L. M., Srinivasan, K., and Somayaji, C., An Examination of Regenerative Organic Rankine Cycles Using Dry Fluids, *Applied Thermal Engineering*, vol. 28, pp. 998–1007, 2008.



Karthikeyan Palanisamy is a Master's student at the Mechanical Engineering Department of the University of British Columbia, working on the modeling of agglomerate formation in bitumen processing. He received his Bachelor's of Technology (B.Tech.) degree with honors from the Indian Institute of Technology (IIT) Bhubaneswar in 2013. He had the privilege of working under Dr. Markides on the NIFTE during the summer of 2012. His research interests cover the modeling of transport phenomena, CFD and heat transfer, waste heat recovery, automotive engineering and manufacturing, robotics, and intelligent systems.



Aly I. Taleb is a Doctoral student in the Clean Energy Processes Group at the Department of Chemical Engineering of Imperial College London. He received the title of Diplom-Ingenieur (Dipl.-Ing.) in mechanical engineering from the Technische Universität München (TUM) in Munich, Germany, in 2011. Afterward, he worked for one year for BMW as a design engineer in the area of electric vehicles. His research revolves around energy efficiency and waste heat recovery, organic Rankine cycles and unsteady heat engines for low-grade heat conversion, and organic working fluids.



Christos N. Markides is a Senior Lecturer in Clean Energy Processes and heads the Clean Energy Processes (CEP) research group at the Department of Chemical Engineering, Imperial College London. He was also one of the co-founders and acted as Technical Director of Thermofluidics Ltd., a spin-off company that was created in 2006 to develop and commercialize the NIFTE technology. He studied for his B.A., M.Eng., and Ph.D. degrees at the Department of Engineering of the University of Cambridge. He graduated with a first class B.A. degree (with honors) in Engineering in 2000. The following year he completed his Master's degree in the fields of fluid mechanics and thermodynamics, for which he obtained a distinction. He was awarded a Ph.D. in energy technologies in 2006. His current research interests include the thermodynamics of and heat transfer effects in innovative unsteady devices and machines, with applications in energy (heat and power) conversion, integration, and storage, in particular for the efficient utilization of low-grade (solar or waste) heat.

Downloaded by [Imperial College London Library] at 09:18 20 April 2015